LETTER

Porosimetry and packing morphology of vertically aligned carbon nanotube arrays via impedance spectroscopy

To cite this article: Heena K Mutha *et al* 2017 *Nanotechnology* **28** 05LT01

View the article online for updates and enhancements.

Related content

- Capacitance behavior of nanostructured - MnO2/C composite electrode using different carbons matrix
  Van Man Tran, An The Ha and My Loan Phung Le

- Recent progress and performance evaluation for polyaniline/graphene nanocomposites as supercapacitor electrodes
  Mahmoud Moussa, Maher F El-Kady, Zhiheng Zhao et al.

- Low dimensional carbon and MXene based electrochemical capacitor electrodes
  Yeoheung Yoon, Keunsik Lee and Hyoyoung Lee

Recent citations

- Yangying Zhu *et al*

- Characterization of Bone Char and Carbon Xerogel as Sustainable Alternative Bioelectrodes for Bioelectrochemical Systems
  E. D. Isaacs-Páez *et al*

- A general model for the impedance of batteries and supercapacitors: The non-linear distribution of diffusion times
  Emanuele Quattrocchi *et al*

IOP ebooks™

Bringing you innovative digital publishing with leading voices to create your essential collection of books in STEM research.

Start exploring the collection - download the first chapter of every title for free.

Letter

Porosimetry and packing morphology of vertically aligned carbon nanotube arrays via impedance spectroscopy

Heena K Mutha[1], **Yuan Lu**[2], **Itai Y Stein**[1], **H Jeremy Cho**[1], **Matthew E Suss**[3], **Tahar Laoui**[4], **Carl V Thompson**[2], **Brian L Wardle**[5,6] and **Evelyn N Wang**[1,6]

[1] Mechanical Engineering, Massachusetts Institute of Technology, Cambridge, MA 02139, USA
[2] Materials Science, Massachusetts Institute of Technology, Cambridge, MA 02139, USA
[3] Mechanical Engineering, Technion Israel Institute of Technology, Technion City, Haifa, 3200003, Israel
[4] Mechanical Engineering, King Fahd University of Petroleum and Minerals, Dhahran, 31261, Saudi Arabia
[5] Aeronautics and Astronautics, Massachusetts Institute of Technology, Cambridge, MA 02139, USA

E-mail: wardle@mit.edu and enwang@mit.edu

CrossMark

Abstract

Vertically aligned one-dimensional nanostructure arrays are promising in many applications such as electrochemical systems, solar cells, and electronics, taking advantage of high surface area per unit volume, nanometer length scale packing, and alignment leading to high conductivity. However, many devices need to optimize arrays for device performance by selecting an appropriate morphology. Developing a simple, non-invasive tool for understanding the role of pore volume distribution and interspacing would aid in the optimization of nanostructure morphologies in electrodes. In this work, we combined electrochemical impedance spectroscopy (EIS) with capacitance measurements and porous electrode theory to conduct *in situ* porosimetry of vertically aligned carbon nanotube (VA-CNT) forests non-destructively. We utilized the EIS measurements with a pore size distribution model to quantify the average and dispersion of inter-CNT spacing (Γ), stochastically, in carpets that were mechanically densified from 1.7×10^{10} tubes cm^{-2} to 4.5×10^{11} tubes cm^{-2}. Our analysis predicts that the inter-CNT spacing ranges from over 100 ± 50 nm in sparse carpets to sub 10 ± 5 nm in packed carpets. Our results suggest that waviness of CNTs leads to variations in the inter-CNT spacing, which can be significant in sparse carpets. This methodology can be used to predict the performance of many nanostructured devices, including supercapacitors, batteries, solar cells, and semiconductor electronics.

S Online supplementary data available from stacks.iop.org/nano/28/05LT01/mmedia

Keywords: porosimetry, aligned nanowires, carbon nanotubes, electrochemical impedance spectroscopy, supercapacitors

(Some figures may appear in colour only in the online journal)

1. Introduction

Vertically aligned one-dimensional (1D) nanostructures such as tubes, rods, and wires have been gaining an immense

amount of attention for use in electrochemical systems, electronics, optoelectronics, sensing, and solar cells [1]. Polymeric, semiconductor, and crystalline nanowires, as well as vertically aligned carbon nanotube (VA-CNT) forests are being investigated as high-performance materials in these broad applications. Numerous break-throughs in synthesis have made it possible to grow high aspect ratio nanowires [1–3], with the promise of large device scalability [1, 4, 5], leading to the use in many applications that require high gravimetric or volumetric surface area. In electrochemical systems, a large effective surface area results in a sizable density of ion adsorption sites for large double layer capacitance [6] in supercapacitors and capacitive deionization devices, or a great number of sites for redox reactions in fuel cells [7], artifical photosynthesis [8] and batteries [9–12]. In addition, 1D nanostructure arrays have minimally tortuous geometries, which can lead to significant power densities due to the presence of many easily accessible electrolyte pathways from the bulk solution to the surface of the electrodes [13]; VA-CNT electrodes have demonstrated up to 20 times faster charging rates compared to arbitrarily deposited CNTs [14]. In solar cell applications, vertically aligned nanowire arrays with interspacings on the order of the wavelength of light can yield high light absorption due to long optical lengths and photonic effects [1, 4, 15–17].

However, 1D arrays tend to be sparse, and increasing packing density to improve device performance has been of interest in many applications [2, 16, 18]. In solar cells, semiconductor nanowires have shown a dependency of interspacing on the short circuit current, where the highest current is achieved between 50–300 nm interspacings [4]. Similarly, in VA-CNT supercapacitors, densification [19] has led to volumetric capacitance gains directly proportional to the degree of packing, while gravimetric capacitance is invariant [20, 21]. However, the rate capability of an electrode is dependent on the pore conductance, which is proportional to the cross-sectional area of the pore [22], and optimal pore sizes have been found in the range of sub-2 to tens of nanometers [23]. This prompts the question of how to design nanowire arrays to optimize volumetric surface area through increased packing without compromising performance. In order to model and design 1D nanostructure arrays, it becomes critical to have the capability to measure the interspacing to match device capability with material synthesis.

In sparse 1D nanostructure arrays, typically scanning electron microscopy is used to characterize the diameter of pores and interspacing [2, 3, 5, 8]. In VA-CNT forests where the features are finer, many techniques are used to characterize the alignment of forests and the diameter of nanotubes [24], but few quantify the interspacing. Typically, the surface area, diameter, and volume of pores in VA-CNT forests are calculated using Brunauer–Emmett–Teller (BET) theory (e.g., gas adsorption isotherm analysis). A limitation however is that gas adsorption measurements tend to include both the inner and outer surfaces of the nanotube [25], though typically only the outer surface area is exposed to electrolytes [13]. In addition the quantitative pore size distribution from BET analysis is typically accurate from 1.5–15 nm [26], a

smaller range than predicted CNT interspacings. In VA-CNT membranes, it is possible to measure the pore size distribution using varying diameter solute rejection [27], but this approach is vulnerable to leaks in the membrane. Another approach for estimating interspacing has been based on calculating the mass density, and average CNT characteristics such as height, inner diameter, and outer diameter in a sample (measured through transmission and scanning electron microscopy (TEM and SEM, respectively) characterization) [20, 25]. These values have been used either by assuming an ideal packing geometry [19, 20], or more recently with a continuous coordination number model [28], to predict an approximate average pore inter-CNT spacing, Γ. While these theories can provide an approximate value of Γ, they assume each nanotube is perfectly straight and therefore do not predict a large dispersion of Γ in a forest. However, recent stochastic modeling of VA-CNT forest growth has suggested that waviness of the nanotubes, leads to large dispersion [29], and is reduced as a function of increasing packing proximity [30]. More recently, SEM imaging of a cross-section has been used with image analysis to define the front-most plane based on the brightness of a CNT, to measure spacings along cross-sections of carpets [28]. However, these methods are limited to small regions of the sample (micrometer range) [31], and may not capture the macroscopic properties of the forest. In addition these methods are time-consuming and highly destructive, which prevent samples whose morphologies were characterized from being used in subsequent experiments.

In this letter, we show that electrochemical impedance spectroscopy (EIS) can offer *in situ* non-destructive characterizations to determine the morphology of 1D nanostructure arrays and Γ over the entire measured sample. In this study we use VA-CNT forests which provide the ability to easily vary the packing density through mechanical densification [19] leading to a reduction in Γ. Using a simple three-electrode beaker system, we conducted electrochemical experiments on VA-CNT carpets. We determined the double layer capacitance, C_{dl}, of the CNT surface using cyclic voltammetry (CV) to obtain a capacitive operating voltage window and potentiostatic experiments to measure charge. We then used EIS to study the frequency response of the electrodes. By combining these measurements with a mathematical model for porous electrodes, we were able to obtain the average, Γ_{μ}, and the dispersion (i.e., standard deviation), σ, of the inter-CNT spacing Γ of VA-CNT carpets of varying densities. This approach can be extended to other 1D nanostructure arrays in order to quantify the average and dispersion of interspacings and predict specific device performance.

2. Methods

We synthesized and densified VA-CNT forests to study samples of varying porosity. The sample capacitance and frequency response were measured using CV, potentiostatic testing, and impedance spectroscopy in order to analyze the inter-CNT spacing.
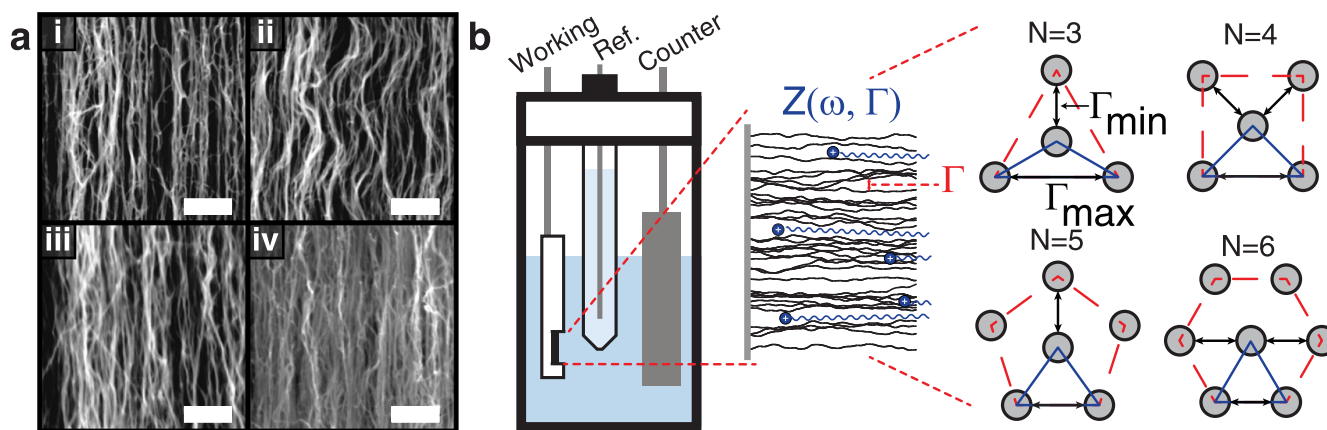
Figure 1. VA-CNT porosimetry study utilizing impedance spectroscopy ($Z(\omega)$) to assess morphology. (a) SEM images of VA-CNT forests of varying volume fractions (i) 1%, (ii) 2%, (iii) 5%, (iv) 10%. Scale bar is 0.5 μm. (b) (left) A three electrode beaker experiment is used to study the inter-CNT spacing, Γ, in a forest. (middle) The impedance Z response is a function of the voltage input frequency ω and Γ. (right) The morphology is modeled from theoretical coordinations N where Γ of the pore is an average of the minimum and maximum inter-CNT spacing in a given unit cell.

2.1. VA-CNT synthesis and densification

We synthesized $1 \times 1 \times 0.1$ cm VA-CNT carpets using chemical vapor deposition, using the procedure described by Stein *et al* [31]. Synthesis and characterization details of the multi-walled VA-CNT array are provided in the supplementary material. The volume fraction V_f of a forest is defined as the ratio of CNT volume to the total volume. Typically, the initial forest has a V_f of ~1% [32]. Through mechanical densification [19], we increased the density of grown forests from 1–3×10^{10} tubes cm^{-2} to 4.5×10^{11} tubes cm^{-2}, i.e., up to $V_f \sim 25\%$. Figure 1(a) shows with increasing V_f, both Γ in the forest and w of the CNTs is reduced, similar to samples used in previous work [19, 31, 32]. With these samples, we can study the change in Γ_μ and σ with a large range of densities.

2.2. Three-electrode electrochemical testing

We conducted electrochemical experiments using a three electrode set up with a VA-CNT forest working electrode, Ag/AgCl reference electrode (Beckman Coulter, 3.5 M KCl), and an oversized 2×5 cm Pt foil (Sigma-Aldrich) counter electrode all immersed in 1 M NaCl solution (figure 1(b)). See supplementary material for further experimental set-up details and additional experiments conducted in 500 mM NaCl.

We used CV at a ramp rate of 10 mV s^{-1} to determine the capacitive (e.g. non-Faradaic) window for EIS experiments. We then conducted potentiostatic testing to determine the capacitance of each sample. We applied a square wave, with a positive potential varying from 0.05 to 0.5 V, discharged at 0 V versus Ag/AgCl for 2 min while the current response was measured and subsequently integrated to calculate charge. From measuring charge as a function of voltage, we determined the steady state capacitance and normalized by the total CNT surface area to determine C_{dl}. Finally, we conducted EIS measurements at half-cell voltages between 0 and 0.5 V versus Ag/AgCl to study the frequency

response between 10 kHz and 100 mHz of the VA-CNT electrodes.

3. Results and discussion

We used three-electrode measurements to analyze the C_{dl} and frequency response of the electrodes. We then used a modified porous distribution model described here to extract values for the mean and dispersion of the inter-CNT spacings in varying density VA-CNT forests.

3.1. Electrochemical measurements

CV scans at 10 mV s^{-1} showed that VA-CNT electrodes behave capacitively from -0.5 to 0.5 V versus Ag/AgCl (figure 2(a)). The volumetric capacitance of the electrodes scales with the density of the CNTs, from 0.47 F cm^{-3} at $V_f = 1\%$ up to 8.1 F cm^{-3} at $V_f = 15.8\%$. This result indicates that while increasing densification of the carpets, the gravimetric capacitance is maintained. The C_{dl} varied between 7–12 μF cm^{-2} (figure 2(b)), independent of volume fraction. These values are comparable to double layer capacitances in literature ranging from 6–50 μF cm^{-2} [14, 20, 33–37]. Due to the known variations of C_{dl} in carbon materials which is dependent on surface chemistry, crystal structure, and electrolyte [13], it is essential to obtain an experimentally characterized value that can be subsequently used in a porosimetry model (described next) rather than literature values. The Nyquist plot (figure 2(c)) shows the impedance response for varying volume fractions from 1%–15%. The high frequency response has the 45° slope, characteristic of porous electrodes [22]. In addition, the impedance increases with higher volume fraction as expected from the increasing ionic resistance with a smaller Γ. In the low frequency regime, the impedance slope tends toward a value $< 90°$, suggesting that there is a sizable variation of Γ in the forest [38].
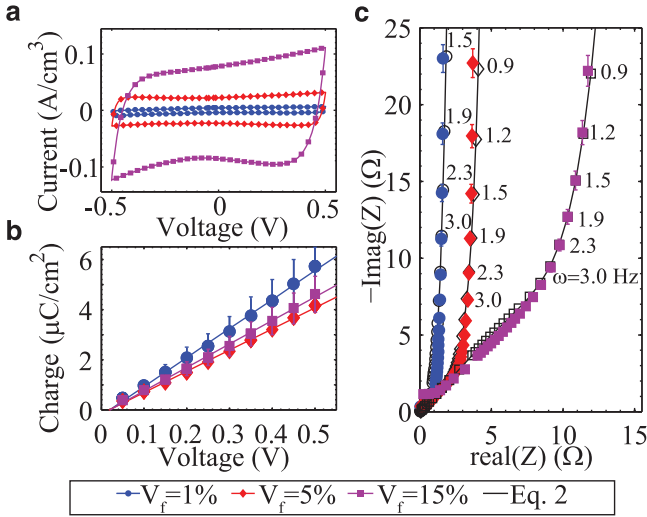
Figure 2. Electrochemical characterizations. (a) Cyclic voltammo-grams (1 M NaCl and 10 mV s^{-1}) indicating a capacitance window from 0 to 0.5 V versus Ag/AgCl. (b) DC charge versus potential shows that sample capacitance varies between 7–12 μF cm^{-2}. (c) Nyquist plot of EIS data and model at 0 ± 5 mV. Data in colored symbols compared to the porosimetry model fit (equation (2)) given by open symbols and black lines (corresponding frequencies of select data points annotated). Here fit is shown for coordinate number $N = 3$ (similar results for other N).

3.2. Porosimetry analysis

To use the electrochemical measurements to determine the morphology of the VA-CNT carpets, we extended de Levie's transmission line model for porous electrodes [22], through which EIS can be used to analyze the pore structure. In the de Levie model, an applied sinusoidal potential with frequency ω across a single cylindrical pore, generates an electrical impedance response, Z_p, given as

$$Z_p = \frac{1}{\pi\sqrt{(2\kappa r^3 \omega C_{dl} j)}} \coth l_p \sqrt{\frac{2j\omega C_{dl}}{\kappa r}}, \tag{1}$$

where r is the radius, l_p is the pore length, capacitance C, in an electrolyte with conductivity κ, and the double layer capaci-tance $C_{dl} = C/A_{pore}$ where A_{pore} is the electrode surface area of the pore. In this model, we assume the the CNT resistivity is negligible because the conductivity of electrolyte in the pore is much lower than CNT conductivity. For a porous electrode with n uniform pores, the total impedance is then simply $Z = Z_p/n$. However, a system that has a distribution of pore sizes will have a non-uniform impedance response [38]. The total impedance response, Z_{tot}, for a porous elec-trode with a distribution of radii given by a mean radius μ_r and dispersion σ_r described by a probability density function f_{pdf} [38] is

$$Z_{tot} = \left(n \int_0^\infty \frac{f_{pdf}(r_o : \mu_r, \sigma_r)}{Z_p(r_o)} dr_o \right)^{-1}. \tag{2}$$

In this treatment, there are three free parameters: μ_r, σ_r, and n, and it has been shown that this leads to many possible solutions due to the ability to vary both the total pore volume and σ_r for a given μ_r [39]. For many porous electrode mate-rials such as activated carbon where the total number of pores is unknown, this can lead to an infinite number of solutions [40]. However, in the case of any brush electrode, where the total number of wires can be calculated based on mass, we can determine n by assuming a coordination geometry. Pre-vious work [28] suggests that the coordination of the VA-CNT forests can range from hexagonal packing with defects to cubic, pentagonal, or ideal hexagonal packing, with coor-dination numbers $N = 3, 4, 5, 6$ respectively (figure 1(b)), and a corresponding number of CNTs per pore, $M_{cnt}(N)$. Therefore, by assuming N for the VA-CNT forest, we can calculate the total number of pores, n, by dividing the number of CNTs by M_{cnt}, and eliminate n as a free parameter. Finally, in order to properly represent VA-CNT forests as cylindrical pores given in equation (2), we projected the cross-sectional area of the pore and the double layer capacitance from a coordinate morphology to a cylindrical pore. Please see the online supplementary material for further detail. The pore double layer capacitance is then

$$C_{dl,pore} = \frac{C_{dl} M_{cnt} A_{cnt}}{A_{pore}(r_o)}, \tag{3}$$

where A_{cnt} is the outer surface area of an average CNT. Therefore, the impedance response and subsequently the calculated inter-CNT spacing are dependent on the CNT outer diameter, which has also been shown in theoretical analysis [28]. While previous VA-CNT porosimetry work has assumed $M_{cnt} = 1$ [14], the coordinate analysis suggests that M_{cnt} varies between 1.5 and 3. This result indicates that the CNT densities were overestimated in the earlier work.

Porosimetry was obtained in this study using equation (2) where four possible N values were used to establish the range of possible interspacings and to give a more accurate description for varying densities of forests. We selected a Gaussian distribution for f_{pdf}, based on the interspacings characterized at high volume fractions from past work with BET [41], solute rejection [27] and stochastic modeling [29]. We used the C_{dl} measured from potentiostatic testing as an input for each sample when conducting the porosimetry analysis. Figure 3 shows the calculated Γ and σ for coordinate numbers $N = 3$ and $N = 6$, which represents the upper and lower bounds of possible interspacings in the forest. For comparison, we also plot the results of a stochastic CNT model [29], where CNT growth is simulated for a given N and w to account for non-idealities in the forest. The as grown 1% V_f forests had a Γ_μ of 77–110 nm with a σ of 40–60 nm. As the samples were densified to 26% V_f, Γ_μ was reduced to 9–15 nm with σ of 4–5 nm. The average inter-CNT spacing decreased with densification, but also the sample uniformity increased. At low V_f, σ was very large, suggesting that there is not a strong packing coordination in the forest, and there is high dispersion in the nanotube Γs which is also consistent with the large spatial inhomogeneities recently observed
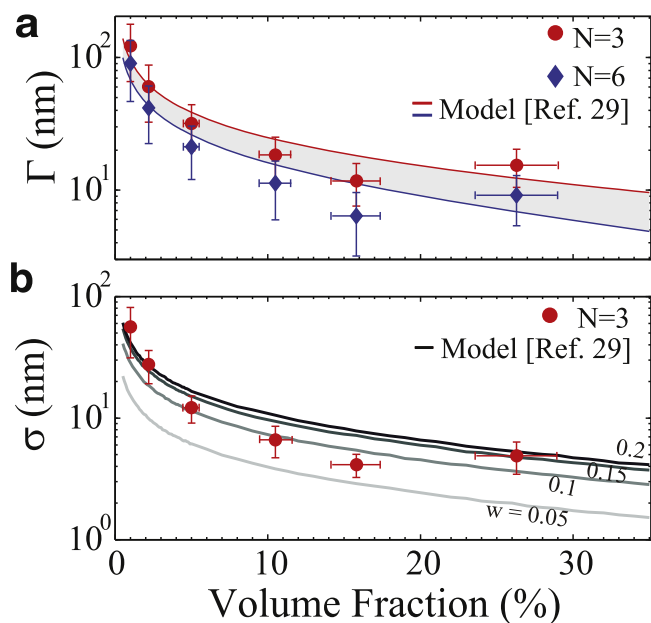
Figure 3. Inter-CNT spacings of VA-CNT forests compared to stochastic model [29]. (a) Γ calculated from EIS and compared to theory given by solid lines [29]. Data shown for $N = 3$ and $N = 6$ fittings (points are average Γ_μ, vertical error bars represent the dispersion σ). Gray region shows span of Γs for $N = 3$ to $N = 6$. (b) σ for varying volume fractions. Contours depict waviness, w, of CNTs, calculated from the model [29]. Plot shown here for $N = 3$ (similar plots in supplementary material for $N = 4, 5, 6$). Vertical error bars are uncertainty of σ in porosimetry analysis.

using 3D quantitative electron tomography [40]. At higher V_f, the array tends towards hexagonal packing when compared to the stochastic model [29] though the dispersion is such that the sample likely had a mixture of packing order. The stochastic model trend diverged from the impedance results with higher V_f, which may be due to bundling or buckling of CNTs during the densification process, leading to greater inhomogoneities. When comparing these results to previous SEM characterizations [28], we found that the EIS approach predicted larger Γ_μ and σ of the interspacing than what was observed optically in a 2D image. This discrepancy may be due to the electrochemical approach providing measurements over the entire forest rather than a cross-section, or that the waviness of the CNT samples lead to a larger standard deviation in spacings than what can be measured optically. The results suggest that a bulk measurement such as this impedance approach is more comprehensive.

Finally, we compared the dispersion calculated in the impedance analysis to stochastic modeling of CNTs with a specified waviness. Figure 3(b) shows that the impedance analysis predicts a large σ of the VA-CNT array at low V_f, and it tends to decrease with increasing V_f. The agreement between calculated σ and stochastic model [29], suggests this trend may be due to decreasing waviness of CNTs in the forest. These observations are also in line with qualitative observations made from SEM imaging in figure 1(a), and quantified recently by other groups [42]. However, at very

high densification, we observed a deviation from this trend, which indicates that there may be other effects (such as buckling) that can contribute towards higher tortuosity. Accordingly, for sparse VA-CNT electrochemical devices, it can be important to model the electrode as having a distribution of interspacings due to the waviness of the CNTs, in order to accurately predict the power density. However, at high V_f ($>15\%$), waviness effects may be negligible, and the system can be modeled more similarly to pillars, assuming that there are no other inhomogeneities in the forest. In addition, the porosimetry results derived here can be used to predict the power performance of similar electrodes in other concentrations and species of electrolytes. This analysis can extend a simple beaker supercapacitor experiment to modeling the performance of batteries, fuel cells and desalination devices with more complex kinetics based on the geometries ascertained via EIS and transmission line models.

4. Conclusions

This study presents an *in situ*, non-destructive method to determine the morphology and porosimetry of VA-CNT forests through EIS. We showed through careful analysis of electrochemical techniques we can obtain information on Γ_μ and σ of electrodes based on the response in simple beaker experiments. Our results showed that densified carpets have increased volumetric capacitance and increased CNT alignment, which can enhance the overall performance of a VA-CNT electrode. This technique can be used to complement electrochemical investigations to correlate experimental findings with physical modeling. In the future, this method can be applied to a variety of 1D nanostructure arrays with a range of densities to predict electrode performance based on interspacing and alignment of the structures. We believe that the use of this technique will lead to greater insight into the relationship between structural properties of 1D nanostructure arrays and device performance.

References

[1] Dasgupta N P, Sun J, Liu C, Brittman S, Andrews S C, Lim J, Gao H, Yan R and Yang P 2014 *Adv. Mater.* **26** 2137–84

[2] Wu W Q, Rao H S, Feng H L, Chen H Y, Kuang D B and Su C Y 2014 *Nano Energy* **9** 15–24

[3] Ghoshal T, Senthamaraikannan R, Shaw M T, Holmes J D and Morris M A 2014 *Adv. Mater.* **26** 1207–16

[4] Kempa T J, Day R W, Kim S K, Park H G and Lieber C M 2013 *Energy Environ. Sci.* **6** 719–33

[5] Gazquez G C, Lei S, George A, Gullapalli H, Boukamp B A, Ajayan P M and ten Elshof J E 2016 *ACS Appl. Mater. Interfaces* **8** 13466–71

[6] Simon P and Gogotsi Y 2008 *Nat. Mater.* **7** 845–54

[7] Xia Z, Wang S, Jiang L, Sun H and Sun G 2014 *J. Power Sources* **256** 125–32

[8] Huang Q, Kang F, Liu H, Li Q and Xiao X 2013 *J. Mater. Chem.* A **1** 2418–25

[9] Dörfler S, Hagen M, Althues H, Tübke J, Kaskel S and Hoffmann M J 2012 *Chem. Commun.* **48** 4097–9

[10] Gohier A, Laïk B, Kim K H, Maurice J L, Pereira-Ramos J P, Cojocaru C S and Van P T 2012 *Adv. Mater.* **24** 2592–7

[11] Li S, Luo Y, Lv W, Yu W, Wu S, Hou P, Yang Q, Meng Q, Liu C and Cheng H M 2011 *Adv. Energy Mater.* **1** 486–90

[12] Evanoff K, Khan J, Balandin A A, Magasinski A, Ready W J, Fuller T F and Yushin G 2012 *Adv. Mater.* **24** 533–7

[13] Signorelli R, Ku D C, Kassakian J G and Schindall J E 2009 *Proc. IEEE* **97** 1837–47

[14] Ghosh A, Le V, Bae J and Lee Y 2013 *Sci. Rep.* **3** 2939

[15] Jean J, Chang S, Brown P R, Cheng J J, Rekemeyer P H, Bawendi M G, Gradečak S and Bulović V 2013 *Adv. Mater.* **25** 2790–6

[16] Liu C, Dasgupta N P and Yang P 2014 *Chem. Mater.* **26** 415–22

[17] Docampo P *et al* 2013 *J. Mater. Chem.* A **1** 12088–95

[18] Ryu W H, Yoon J H and Kwon H S 2012 *Mater. Lett.* **79** 184–7

[19] Wardle B L, Saito D S, García E J, Hart A J, de Villoria R G and Verploegen E A 2008 *Adv. Mater.* **20** 2707–14

[20] Futaba D N, Hata K, Yamada T, Hiraoka T, Hayamizu Y, Kakudate Y, Tanaike O, Hatori H, Yumura M and Iijima S 2006 *Nat. Mater.* **5** 987–94

[21] Lachman N, Xu H, Zhou Y, Ghaffari M, Lin M, Bhattacharyya D, Ugur A, Gleason K K, Zhang Q M and Wardle B L 2014 *Adv. Mater. Interfaces* **1** 1400076

[22] de Levie R 1964 *Electrochim. Acta* **9** 1231–45

[23] Burke A 2007 *Electrochim. Acta* **53** 1083–91

[24] Ren Z, Lan Y and Wang Y 2013 *Aligned Carbon Nanotubes* (Berlin: Springer) (doi:10.1007/978-3-642-30490-3)

[25] Stein I Y, Lachman N, Devoe M E and Wardle B L 2014 *ACS Nano* **8** 4591–9

[26] Gregg S J and Sing K 1967 *Adsorption, Surface Area, and Porosity* (New York: Academic) (doi:10.1002/bbpc.19820861019)

[27] Lee K J and Park H D 2016 *J. Membr. Sci.* **501** 144–51

[28] Stein I Y and Wardle B L 2013 *Phys. Chem. Chem. Phys.* **15** 4033–40

[29] Stein I Y and Wardle B L 2016 *Phys. Chem. Chem. Phys.* **18** 694–9

[30] Stein I Y, Lewis D J and Wardle B L 2015 *Nanoscale* **7** 19426–31

[31] Stein I Y and Wardle B L 2014 *Carbon* **68** 807–13

[32] Lee J, Stein I Y, Devoe M E, Lewis D J, Lachman N, Kessler S S, Buschhorn S T and Wardle B L 2015 *Appl. Phys. Lett.* **106** 053110

[33] Niu C, Sichel E K, Hoch R, Moy D and Tennent H 1997 *Appl. Phys. Lett.* **70** 1480–2

[34] Frackowiak E, Metenier K, Bertagna V and Beguin F 2000 *Appl. Phys. Lett.* **77** 2421–3

[35] An K H *et al* 2001 *Adv. Funct. Mater.* **11** 387–92

[36] Du C, Yeh J and Pan N 2005 *Nanotechnology* **16** 350–3

[37] Kim B, Chung H and Kim W 2012 *Nanotechnology* **23** 155401

[38] Song H K, Sung J H, Jung Y H, Lee K H, Dao L H, Kim M H and Kim H N 2004 *J. Electrochem. Soc.* **151** E102–9

[39] Musiani M, Orazem M, Tribollet B and Vivier V 2011 *Electrochim. Acta* **56** 8014–22

[40] Natarajan B, Lachman N, Lam T, Jacobs D, Long C, Zhao M, Wardle B L, Sharma R and Liddle J A 2015 *ACS Nano* **9** 6050–8

[41] Yu M, Funke H H, Falconer J L and Noble R D 2009 *Nano Lett.* **9** 225–9

[42] Lee B, Baek Y, Lee M, Jeong D H, Lee H H, Yoon J and Kim Y H 2015 *Nat. Commun.* **6** 7109